NASA Technical Memorandum 84345



# Supporting Flight-Data Analysis for Space-Shuttle Orbiter Experiments at NASA Ames Research Center

Michael J. Green, Mari P. Budnik, Lily Yang and Matthew P. Chiasson

April 1983



NASA
National Aeronautics and Space Administration

NASA Technical Memorandum 84345

# Supporting Flight-Data Analysis for Space-Shuttle Orbiter Experiments at NASA Ames Research Center

Michael J. Green, Ames Research Center, Moffett Field, California
Mari P. Budnik
Lily Yang, Informatics General Corporation, Palo Alto, California
Matthew P. Chiasson, Foothill College, Los Altos, California

National Aeronautics and
Space Administration

**Ames Research Center**
Moffett Field, California 94035

# SUPPORTING FLIGHT DATA ANALYSIS FOR SPACE SHUTTLE ORBITER EXPERIMENTS AT NASA AMES RESEARCH CENTER

Michael J. Green*
NASA Ames Research Center, Moffett Field, California

Mari P. Budnick† and Lily Yang†
Informatics General Corporation, Palo Alto, California

Matthew P. Chiasson‡
Foothill College, Los Altos, California

## Abstract

The Space Shuttle Orbiter Experiments program is responsible for collecting flight data to extend the research and technology base for future aerospace vehicle design. The Infrared Imagery of Shuttle (IRIS), Catalytic Surface Effects, and Tile Gap Heating experiments sponsored by Ames Research Center are part of this program. The paper describes the software required to process the flight data which support these experiments. In addition, data analysis techniques, developed in support of the IRIS experiment, are discussed. Using the flight data base, the techniques have provided information useful in analyzing and correcting problems with the experiment, and in interpreting the IRIS image obtained during the entry of the third Shuttle mission.

## Introduction

NASA's Orbiter Experiments (OEX) program is responsible for collecting data to extend the aerothermodynamic environment and thermal protection system (TPS) data base for future aerospace-vehicle design. The OEX program currently includes nine experiments that are designed to increase the understanding of the effects of hypervelocity atmospheric entry on a winged reusable vehicle. An overview of the experiments is given in Ref. 1. Ames Research Center (ARC) supports the following three experiments: Infrared Imagery of Shuttle (IRIS), Catalytic Surface Effects (CSE), and Tile Gap Heating (TGH). To provide research-quality flight data for the experiments during the initial shuttle flights, orbiter vehicle OV-102, familiarly known as the Columbia, has been instrumented with thermocouples, pressure transducers, calorimeters, and radiometers. These are part of the Development Flight Instrumentation (DFI). For each of the first five Space Transportation System (STS) flights, measurements during atmospheric entry were recorded and later distributed to researchers working on OEX experiments. In addition, postflight trajectory and atmospheric reconstructions were provided.

Here, we describe the data processing methods that have been developed to convert and merge flight data obtained from various sources, into data required to support the three OEX experiments at ARC. Preflight and postflight supporting data analysis for the IRIS experiment is presented, and is of primary focus. To illustrate its use, the processed data are compared with results from the analyses developed by OEX investigators.

*Research Scientist, Entry Technology Branch, Member AIAA.

†Staff Analyst.

‡Student Intern.



## Data Sources

Data required to support the OEX experiments are supplied by the Johnson Space Center (JSC) and by the Langley Research Center (LaRC), and are transmitted by magnetic tape. Before each STS mission, JSC provides the Instrumentation Program and Components List (IPCL), which contains specific information about each of the 4000 DFI devices, including the more than 300 on the lower surface of the orbiter. The information includes the measurement number, location coordinates, the allowable data range, and units. Periodically, updates are published[2] and incorporated into the list.

After each mission, the flight data are processed as shown in Fig. 1. The usual DFI data flow is shaded in gray: after a landing, tapes from the flight recorder onboard the orbiter are dumped onto backup tapes, which are then sent to JSC. There, the raw analog data are digitized and converted to engineering quantities using experimentally determined calibration-polynomial fits. Finally, data tapes are sent to OEX researchers. If the onboard DFI data are not available, as were the cases for STS-1 and -4, only real-time data telemetered from the orbiter after the blackout period are obtained.

The DFI data received at ARC are from measurements of the Aerothermodynamic and TPS subsystems during entry. The instruments on OV-102 are located primarily on the port side of the lower surface of the vehicle, including the fuselage, wing, elevons, and body flap. They include surface, in-depth, and bondline thermocouples, surface pressure transducers, calorimeters, and radiometers. In general, their accuracy is within ±5%. The measurement data are usually available from Entry Interface (EI), defined as the time when the altitude of the orbiter is 122 km (400 kft), to one hr after touchdown, and have a sample rate of one measurement per second. In this work, main emphasis is given to the 84 surface temperature measurements; their locations are displayed in Fig. 2. Incidentally, note that the axial (x) and spanwise (y) coordinates are nondimensionalized by the orbiter length $L = 32.89$ m and the span $S = 23.87$ m, respectively. This nondimensionalization is used throughout the paper. Each measurement, after being digitized, is recorded as an 8-bit count that is then converted with a calibration polynomial to a temperature. The minimum resolution is 5 K per count, which is well within the reported uncertainty of ±2%.[3]

LaRC provides a post-flight tape containing a best estimated trajectory (LaBET) for the entry from an altitude of 122 km to landing. The methods for trajectory recontruction and atmospheric modeling are described in Refs. 4 and 5, respectively. State variables and free-stream conditions along the entry trajectory of the shuttle are given every

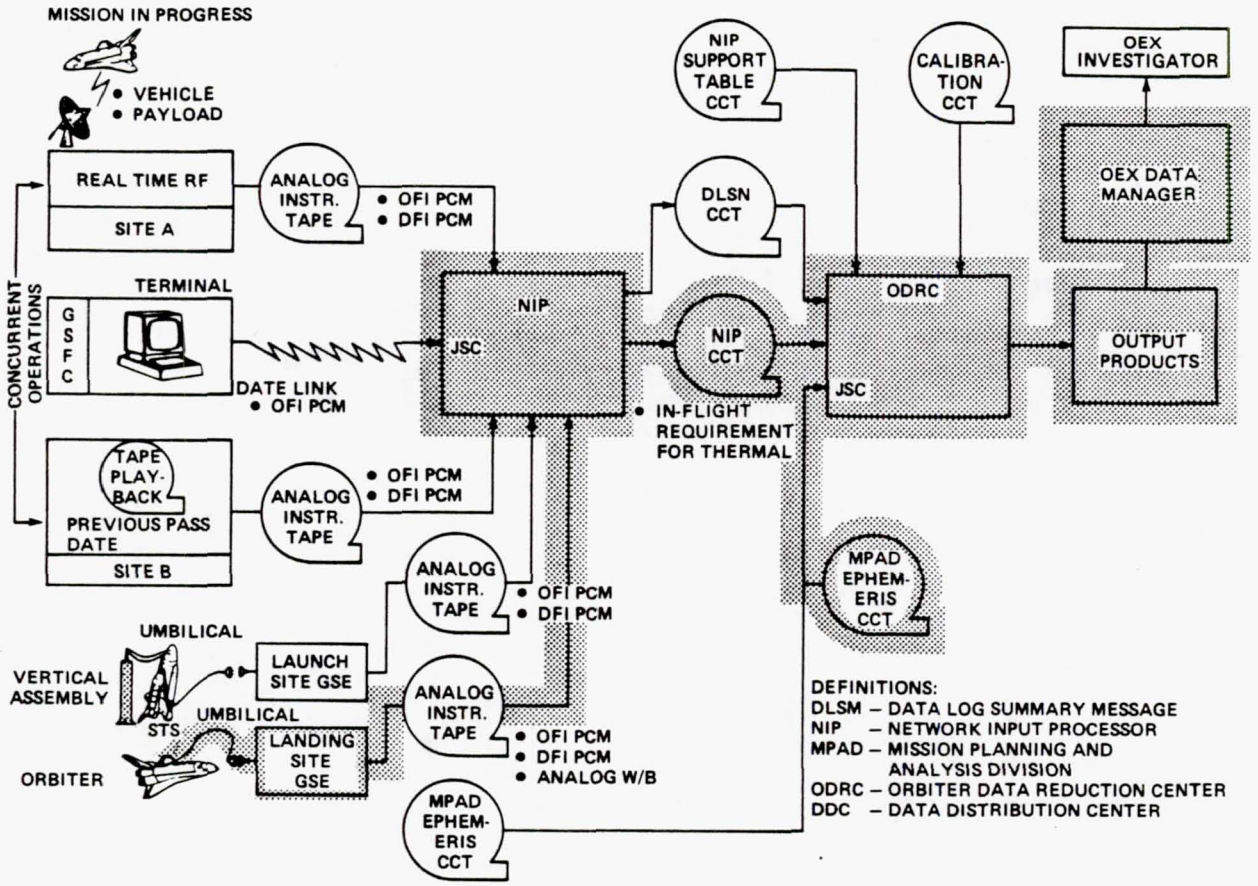


Fig. 1 Flight-data flow.

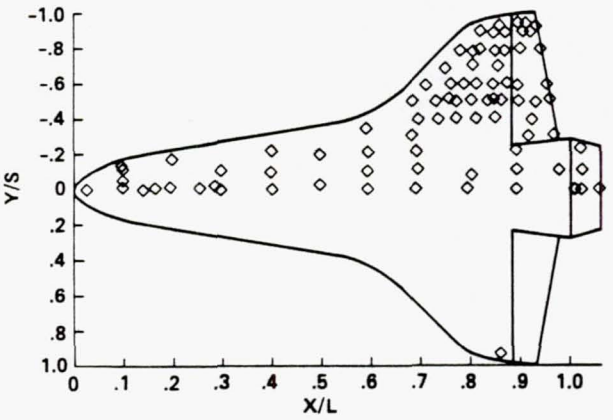


Fig. 2 Lower surface DFI thermocouple locations.

second. The state variables are given relative to a geodetic reference frame.

## Data Processing

Using the information from various sources required software for reading the tapes; for converting the data into a format compatible with the computer resources at ARC; for interrogating the data for bad measurements; for merging necessary data bases; for distributing results to OEX researchers; for archiving results for future research; and for displaying the information in a useful manner. The software development for processing the IPCL was straightforward. Computer programs were written for the CDC 7600 which read the IPCL tape, search and select DFI locations on the orbiter's lower surface, and store them on a permanent disk pack. Whenever necessary, the data can be merged with other data files, such as DFI flight data files when generating plots as a function of location. The software developed for processing the DFI data is more complicated mainly because a bit-by-bit conversion is required from the JSC tape format, which is in UNIVAC display code for a 36-bit single precision word, to an ARC compatible format, which is in CDC internal display for a 60-bit word. We have adapted the conversion algorithm developed for the data information management system at LaRC (Brender, K. D., personal communication, 1980) to our program. Once the data are converted and merged with the IPCL, they are checked to determine if they are in the allowable range for the instrument for archival purposes; if not, they are deleted. Computer programs sort the DFI depending on the application. For instance, the time-dependent surface thermocouple measurements can be separated from the rest of flight data base for more processing. At this point in the data reduction, it is convenient to switch from batch to interactive

processing mode. The data files are transferred from the CDC 7600 to the VAX/11-780 where, for example, plots can be observed from a cathode ray tube screen, and movies generated.

The software for LaBET tape is also straightforward because it is produced on compatible computer equipment at LaRC. The information is stored on a permanent file on the CDC 7600 and is available whenever trajectory or free-stream conditions for a particular STS entry are required.

## IRIS Supporting Data Analysis

### IRIS Experiment

The objective of the IRIS experiment is to determine the temperature distribution on the shuttle's lower and possibly, side surfaces at one instant during its entry trajectory. An accurate temperature distribution, with greater spatial resolution than the DFI measurements, would improve the understanding of such aerothermodynamic phenomena as boundary-layer transition, flow separation and reattachment, and shock interaction. In the experiment, the astronomical telescope, a modified Cassegrainian onboard the Kuiper Airborne Observatory (KAO) C-141 aircraft, obtains an infrared image of the orbiter as it passes through the telescope's field of view. The telescope is located in the fuselage near the front of the left wing. Its movement is restricted to elevation-angle changes in a plane that is perpendicular to the longitudinal axis of the aircraft, it has an aperture diameter of 0.91 m (36 in.). In a nominal encounter, the KAO flies at an altitude 45 km lower than the shuttle and has a boresight separation of about the same distance; the telescope is elevated at 55°.

The IRIS experimental hardware consists of an acquisition telescope, an image-plane assembly, and high-speed data handling equipment. Because the slew rate of the main telescope is too slow for the rapid adjustments required to assure that the hypervelocity shuttle will be in the field of view, a small acquisition telescope is used to acquire the orbiter's emission signal several seconds before the encounter at a distance of some 80 km. It then tracks the orbiter while continually correcting, through a servo system, the elevation angle of the main telescope. The acquisition telescope is mounted on the headring of the main telescope, and rotates azimuthally in a plane perpendicular to the motion of the main telescope. To sense the signal, it has a single Indium Antinomide (InSb) detector covered with a band-pass filter (3-4 μm). The IRIS image-plane assembly, mounted to the KAO at the focal plane, is comprised of a primary linear array of 400 InSb detectors and a secondary array of 200 detectors, located behind and centered relative to the primary, to provide redundant data if the image sweeps through the middle 200 detectors of the primary array. The detectors are covered with a band-pass filter (1.9-2.7 μm). As the image is sweeping through in a direction perpendicular to the arrays, each detector is scanned, in a staggered sequence, every 50 μsec. Data handling hardware amplifies, multiplexes, and digitizes the signal and stores it in computer memory for further data processing. The original IRIS experiment design is described in Ref. 6, and later modifications are presented in Ref. 7.

### Preflight Analysis

The IRIS experiment is currently the only OEX experiment that is remote. This is an advantage since the experiment does not depend, at least directly, on onboard flight instrumentation or data recording equipment. Because data may not be available for many future STS missions, this independence is an important factor. On the other hand, a remote experiment requires much more preflight planning. For the IRIS experiment, for instance, the following two questions, among others related to aircraft communications and logistics, must be answered before an encounter point can be selected: 1) Is this point of scientific interest as far as the aerothermal environment is concerned? and 2) at the required acquisition time, is the strength of the infrared emission from the shuttle within the sensitivity of the acquisition telescope? Both questions can be answered by employing the DFI data base. The first can be answered simply by examining the temperature-time histories of a previous mission with a similar trajectory. An estimate for the time of peak laminar, transitional, or peak turbulent heating can be determined, for example. The second question will be considered next.

Obtaining the signal strength is a two-step process: First, the hemispherical emissive power reradiated from the orbiter's lower surface must be estimated, and then, the fraction of that emission detected by the acquisition telescope is computed. If the surface has an area-averaged temperature $T$ and a gray-body emissivity $\varepsilon = 0.90$ (Ref. 8), the hemispherical emissive power in the infrared wavelength band (3-4 μm) is

$$e = \varepsilon A \int_3^4 e_{\lambda b}(\lambda)\,d\lambda \qquad (1)$$

where Planck's Spectral Energy Distribution,

$$e\lambda b(\lambda) = \frac{2\pi C_1}{\lambda^5 (C_2/e^{\lambda T} - 1)}$$

Here

$$C_1 = 5.9544\times10^{-17}\ \mathrm{Wm}^2$$

$$C_2 = 1.4388\times10^{4}\ \mu\mathrm{mK}$$

and

$$A = 365.9\ \mathrm{m}^2\ ,$$

the orbiter's lower surface area.

The area-averaged temperature can be estimated from the DFI surface temperatures of a previous flight. At the tentative acquisition time, the irregularly distributed temperatures (see Fig. 2) are fit with a smooth surface from which the bivariate-interpolated temperatures can be obtained for uniform incremental areas on the left half of the orbiter's lower surface. Assuming spanwise symmetry, the average temperature over the entire lower surface is approximated as the sum of the interpolated temperatures divided by the sum of the areas. The second-step can now be accomplished. By applying Lambert's Cosine Law for the predicted attitude and orientation of the surface, relative to the boresight direction at acquisition, the

signal strength detected by the acquisition telescope can be calculated.

Postflight Analysis

As the IRIS experiment itself has evolved, so has the supporting postflight data analysis. The original analysis employed a computer-graphics technique for registering the acquired image temperatures to actual physical locations on the orbiter's surface. Using a three-dimensional picture system, the orientation of the orbiter's planform outline relative to the image was obtained by rotating and scaling the outline until it matched the edges of the image. The inverse of the resulting rotation matrix was applied to the image pixel coordinates to map them to those of the orbiter. Once this geometrical registration was accomplished, the Lambertian effect on the emitted flux, because of the curvature of the orbiter's surface, could be accounted for by determining the cosine of the angle between the line-of-sight vector of the telescope and the body-normal vector. Finally, the rectified image thermograph could be compared with the corresponding temperatures at the DFI locations. During the STS-3 entry, an IRIS image was obtained at 16.5 min after EI. The experiment has been attempted on the first four STS flights. A false-color photograph of the unrectified image has been exhibited elsewhere[9]; a black and white version is shown in Fig. 3. Only the right-most 60% of the shuttle was obtained, because the IRIS acquisition telescope and the KAO telescope were misaligned by 3 arcmin.[7] Moreover, since the image swept over the first 71 detectors of the primary array, it missed the secondary array completely and, hence, redundant data were not obtained. In the figure, the image is shown in image-plane coordinates that were derived from the original detector-number and scan-time coordinates.

When the original graphical registration method was applied, the image could not be matched with the orbiter outline satisfactorily; some areas of the image always overlapped the outline. In an effort to resolve this problem, a more rigorous analytical registration method was developed. The IRIS pixel coordinates are projected onto the lower surface of the shuttle using flight orientation information from the shuttle and the KAO aircraft at the time of the encounter. The various coordinate systems used for this projection are shown in Fig. 4a, where $(X_s,Y_s,Z_s)$, $(X_k,Y_k,Z_k)$, $(X_e,Y_e,Z_e)$, and $(X_i,Y_i)$ represent the shuttle, KAO, Earth, and image-plane coordinate systems, respectively. The line-of-sight vector (LOS) points in the direction of the KAO telescope boresight. The orientation of the two vehicles is specified in terms of the Euler angles: yaw, pitch, and roll, denoted by $(\psi,\theta,\phi)$. These angles are defined relative to a particular coordinate system.[10] The shuttle Euler angles are relative to the geodetic Earth coordinate system, in which the x-axis is geographic northward, the y-axis is east (in the local horizontal plane), and the z-axis is downward, normal to the approximate ellipsoid of the Earth. The KAO Euler angles are relative to the geocentric Earth system, in which the x-axis lies in the local meridian plane, the y-axis is east, and the z-axis is toward the gravitational center of the Earth. For convenience in the development, an intermediate Earth system was introduced. The matrix R of the transformation from either vehicle system to the intermediate system is

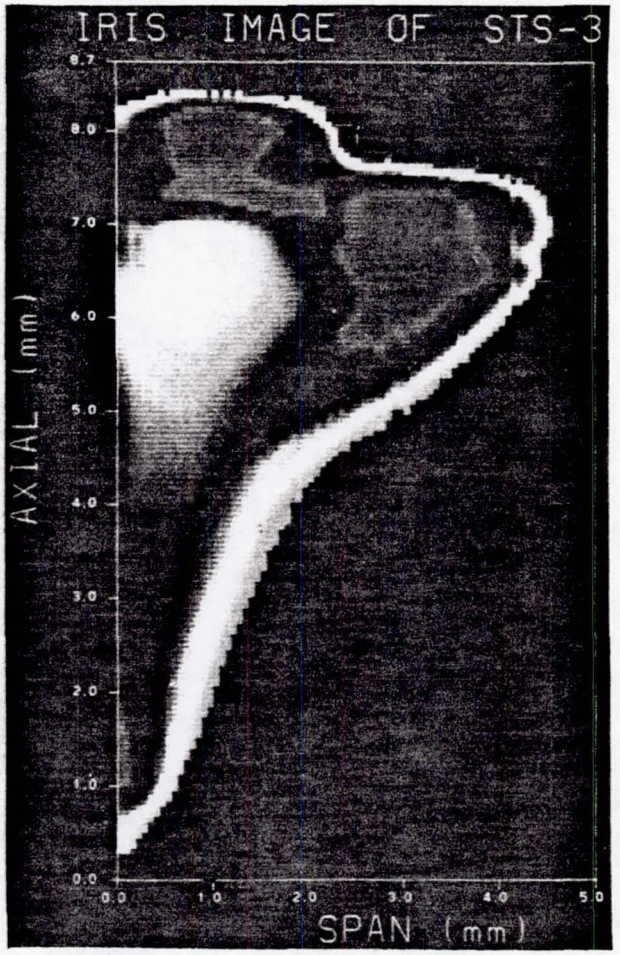


Fig. 3 IRIS image: STS-3.

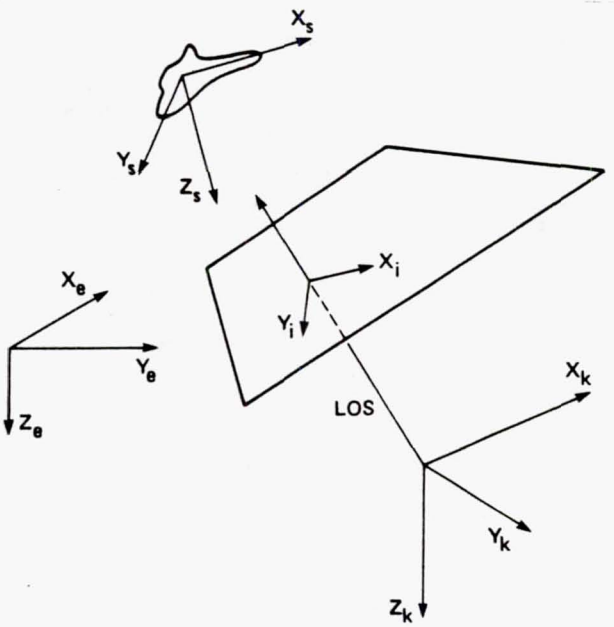


(a) Shuttle, Earth, KAO, and image-plane coordinate systems.

Fig. 4 Analytical registration.

$$R = \begin{pmatrix} \cos\psi\cos\theta & -\sin\psi\cos\phi + \cos\psi\sin\theta\sin\phi & \sin\psi\sin\phi + \cos\psi\sin\theta\cos\phi \\ \sin\psi\cos\theta & \cos\psi\cos\phi + \sin\psi\sin\theta\sin\phi & -\cos\psi\sin\phi + \sin\psi\sin\theta\cos\phi \\ -\sin\theta & \cos\theta\sin\phi & \cos\theta\cos\phi \end{pmatrix}$$

Since this is an orthogonal matrix, the transformation from the Earth system to either vehicle system is simply $R^{-1} = R^t$.

To obtain either of the other two coordinate systems from the Earth system, the following rotations are performed (see Fig. 4b):

1. Rotate the vehicle system about the $Z_e$ axis by $\psi$, creating a new axis system $(X_1,Y_1,Z_1)$.

2. Rotate the $(X_1,Y_1,Z_1)$ system about $(Y_1)$ by $\theta$, creating the $(X_2,Y_2,Z_2)$ system.

3. Finally rotate the $(X_2,Y_2,Z_2)$ system about $(X_2)$ by $\phi$, creating the final vehicle axes $(X_3,Y_3,Z_3)$.

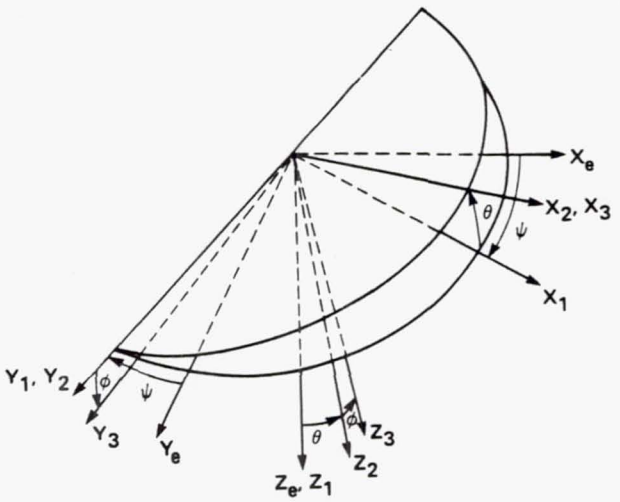


b) Vehicle Euler angles.

Fig. 4 Concluded.

The transformation from the IRIS image plane to the KAO coordinate system is

$$R_k^i = \begin{pmatrix} A_x & B_x & C_x \\ A_y & B_y & C_y \\ A_z & B_z & C_z \end{pmatrix}$$

where $\bar{A}$, $\bar{B}$, and $\bar{C}$ are the x, y, and z axes of the image plane relative to the KAO system. The z axis of the image-plane system is parallel to the LOS vector.

The transformation from the shuttle system to the shuttle x-y plane is

$$R_p^s = \begin{pmatrix} 1 & 0 & -a/b \\ 0 & 1 & b/c \end{pmatrix}$$

where a, b, and c are the LOS direction cosines relative to the shuttle system.

With the preceding transformations, the IRIS image pixel coordinates $(P_i)$ are projected from the image plane to the KAO system, to the Earth system, to the shuttle system, and finally to the shuttle x-y plane $(P_s)$. The corresponding matrix equation is

$$R_p^s R_s^e R_e^k R_k^i P_i = P_s$$

Projecting the planform of the shuttle onto the IRIS image plane requires the inverse of the transformation just given. Here, the matrix for projecting the shuttle outline, in KAO coordinates, onto the image plane is

$$R_i^k = \begin{pmatrix} A_x & A_y & A_z \\ B_x & B_y & B_z \end{pmatrix}$$

where $\bar{A}$ and $\bar{B}$ are the same as before.

Besides the spatial distortion, the IRIS image has, as will be discussed later, thermal anomalies. An effort was undertaken to determine what phenomena caused the distortion and how the image could be restored. In a first effort, it was hypothesized that the image degradation was caused by a defocusing effect in the KAO telescope system. Using the DFI temperatures as control points, an axial temperature distribution $T_F(x)$ at a given spanwise location was generated by interpolation. Assuming that the point spread function that modeled the defocusing effect was a Gaussian density function G, of only the axial variable x, with zero mean and specified standard deviation $\sigma$ (nondimensionalized by L), we determine the defocused temperature distribution $T_C(x)$ as the convolution of $T_F(x)$ and $G(x)$, namely,

$$T_C(x) = \int_{-\infty}^{\infty} T_F(\xi)G(x - \xi)d\xi$$

with

$$G(x) = \frac{1}{\sigma\sqrt{2\pi}} e^{-(1/2)(x/\sigma)^2}$$

The parameter $\sigma$ was varied to best fit the convolved temperature distributions with the IRIS data. Here, spanwise symmetry of the temperature distribution was assumed, because the DFI temperatures are on the left half of the orbiter's lower surface, whereas the partial IRIS image temperatures are mostly on the right.

In another area of IRIS support, a numerical flow-field solution was generated for the IRIS encounter conditions, including the high angle of attack (Balakrishnan, A., Green, M. J., and Davy, W. C., prospective NASA report). The DFI flight data are used to validate the solution which, in

turn, provides information that is needed to understand the effect of the hypersonic shock layer on the emissive flux and thus, on the IRIS image. In the computation, the three-dimensional Navier-Stokes equations for an ideal gas (a perfect gas with a constant ratio of specific heats) are solved in the nose-cap region of the orbiter, a region where the IRIS image is significantly distorted.

## CSE and TGH Data Requirements

Both the CSE and TGH experiments require only a subset of the IRIS DFI data base already discussed. The objective of the CSE experiment is to understand and quantify the effects of surface catalytic efficiency on aerothermal heating.[8] Selected lower-surface tiles are sprayed with an overcoat of highly catalytic material. DFI thermocouple data from these tiles are compared with that from nearby baseline tiles to determine the surface catalyticity. The experiment was flown on the STS-2 through -5 missions. Relevant surface temperature and pressure measurements were provided to the CSE investigators.

The purpose of the TGH experiment is to understand the effect of tile-gap width and depth on gap heating.[11] The experiment has a removable flight-test panel which is instrumented at three different flow-regime locations with one plug and two sidewall in-depth thermocouples. These locations contain a total of one surface and 13 in-depth measurements. After STS-2 and -3, the DFI data was sorted and distributed to the TGH Principal Technologist directly through an interactive computer network. Both CSE and TGH experimenters receive the LaBET data.

## Results and Discussion

### Flight Data

Before discussing results for the OEX experiments, the processed flight data will be exemplified. Using the LaBET[4-5] data, the first five STS trajectories are illustrated in Fig. 5, in terms of the viscous interaction parameter, $M/\sqrt{Re_\infty}$. Here $M$ is the Mach number, and $Re_\infty$ the free-stream Reynolds number, $Re_\infty = \rho_\infty VL/\mu_\infty$, where $L$ is the orbiter length, 32.87 m, and $\mu_\infty$ is based on Sutherland's viscosity law, valid up to an altitude of 90 km. This parameter has been useful as an independent variable when comparing temperature histories from different entry environments.[8] All trajectories are referenced to EI time; actual Greenwich mean times for the five entries are listed in Table 1. The flight environment for the shuttle and KAO at the STS-3 IRIS encounter is given in Table 2.

Examples of the DFI surface-temperature data are shown in Figs. 6a-6e. Temperature-time histories for the only two spanwise symmetric thermocouples (see insert in Fig. 6a) are compared for each STS entry. The thermocouples are located on the wing tips, just ahead of the outboard elevons. Although the data outside of the allowable range of the thermocouple has been removed, it is still somewhat noisy. Before the data are used in an analysis, they are smoothed using interactive processing. Note that for STS-1 and -4, only the data telemetered to ground stations after the blackout perioc are available because of problems with the onboard data-recording systems. For STS-2, -3, and -5, the

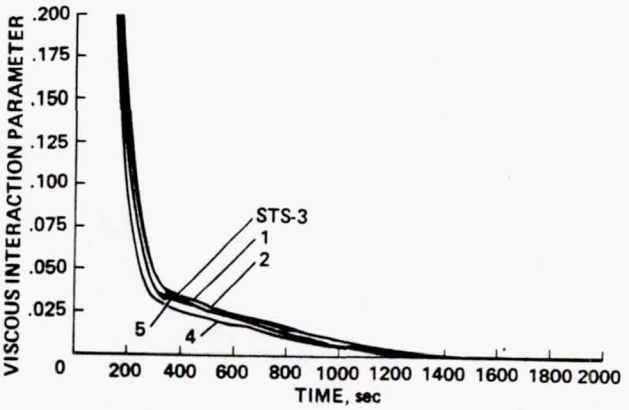


Fig. 5 Viscous interaction parameter histories derived from Langley BET data.

Table 1 STS Entry Times[12]

| STS flight | Date | Day of year | Entry interface,[a] sec | Main landing-gear contact,[a] sec |
|---|---|---|---|---|
| 1 | 04/14/81 | 104 | 64145 | 66057 |
| 2 | 11/14/81 | 318 | 75042 | 76993 |
| 3 | 03/30/82 | 89 | 56084 | 57885 |
| 4 | 07/04/82 | 185 | 56423 | 58180 |
| 5 | 11/16/82 | 320 | 50591 | 52406 |

[a]Greenwich mean time on the given day of year.

Table 2 Flight Environment at IRIS STS-3 encounter

| | |
|---|---|
| **Shuttle trajectory data (Ref. 4)** | |
| Time | 988 sec after EI |
| Altitude | 55.8 km |
| Velocity | 4.30 km/sec |
| Mach number | 13.0 |
| Reynolds number | $4\times10^6$ |
| Angle of attack | 39.66 deg |
| sideslip | -0.13 deg |
| bank | -44.5 deg |
| Elevon deflection | 3 deg |
| Body flap deflection | 7.7 deg |
| Euler angles[a] | |
| Yaw | 51.1 deg |
| Pitch | 26.8 deg |
| Roll | -51.3 deg |
| **Shuttle free-stream conditions (Ref. 5)** | |
| Density | $5.092\times10^{-4}$ kg/m$^3$ |
| Pressure | 39.70 Pa |
| Temperature | 271.6 K |
| **KAO flight data (Fiekowski, P. and Gliniack, J., personal communication, 1982)** | |
| Altitude | 12.5 km |
| Velocity | 0.24 km/sec |
| Euler angles[b] | |
| Yaw | 80.40 deg |
| Pitch | 1.95 deg |
| Roll | 0.25 deg |
| Telescope orientation | |
| Elevation angle | 54.43 deg |
| Azimuth angle | 2.90 deg |

[a]Geodetic coordinate system.
[b]Geocentric coordinate system.

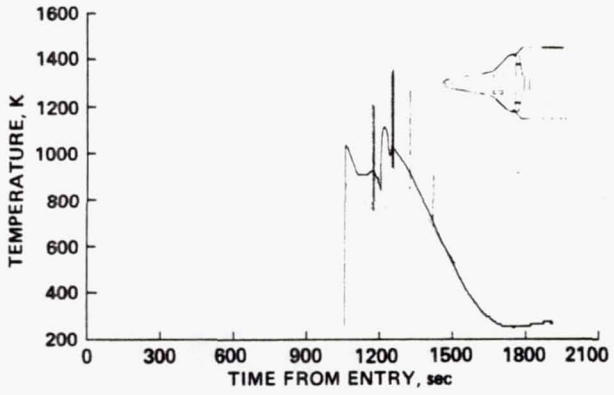


(a) STS-1.

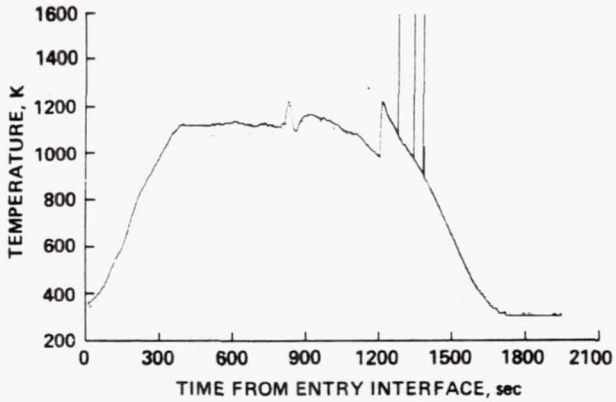


(b) STS-2.

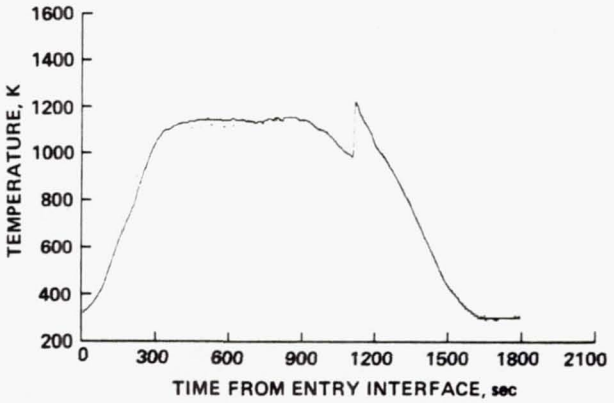


(c) STS-3.

Fig. 6 DFI surface temperature-time histories for spanwise symmetric thermocouples.

profiles are similar. However, because of a longer laminar heating regime than in STS-3, the STS-2 heating load was greater. The profiles for STS-3 and -5 are almost identical, except that in STS-3 boundary-layer transition occurred a minute earlier and, consequently, had higher peak turbulent temperatures. In all the flights, the fully turbulent parts of the profiles are very similar. The temperature blips seen in STS-2 and -5 at 820 sec are

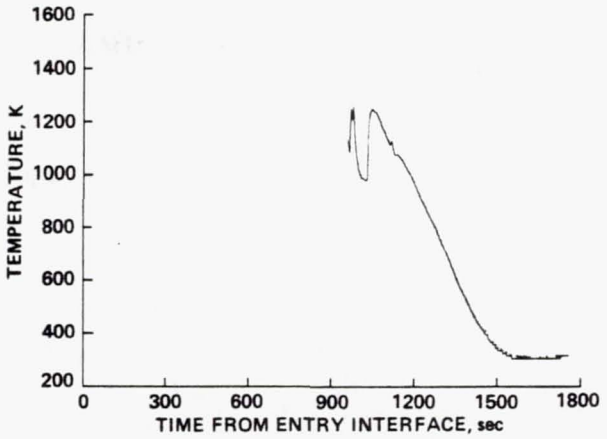


(d) STS-4.

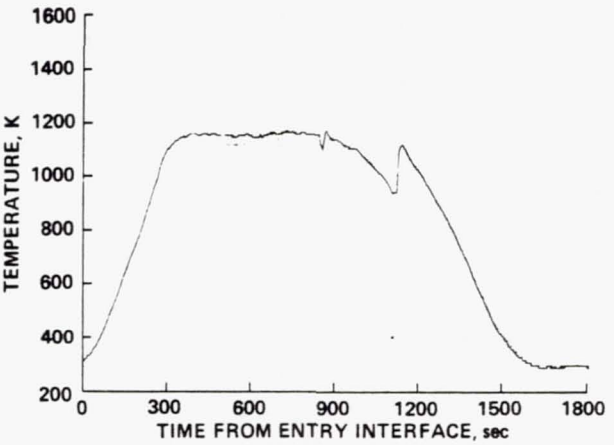


(e) STS-5.

Fig. 6 Concluded.

evidently caused by a 10° peak-to-peak oscillation in angle of attack. These blips appear at all 84 measurement locations.

Qualitatively, the profiles in Figs. 6 are similar to those at other orbiter locations. But at locations nearer the nose, the turbulent heating regime is diminished in both peak temperature and duration relative to that at the wing tip. This is because transition, of course, occurs earlier at the wing tips. Except during the early laminar and the transitional heating periods, based on the only two locations available, the assumption of a spanwise symmetric temperature distribution seems reasonable. In particular, for the STS-3 IRIS encounter at 988 sec, there is only a 20 K difference between the two locations.

## IRIS Experiment Preflight

Figure 7 shows the interpolated surface thermograph using the STS-2 DFI data at 988 sec after EI. The area-averaged temperature is 1020 K. The hemispherical emissive power from the orbiter's lower surface in the acquisition band-pass of 3-4 μm is approximately 3.3 MW. The STS-3 preflight estimate of the signal strength to the acquisition

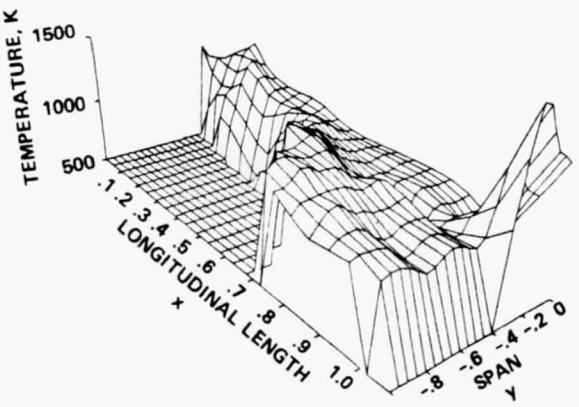


Fig. 7 DFI surface temperature distribution: STS-2, 988 sec after EI.

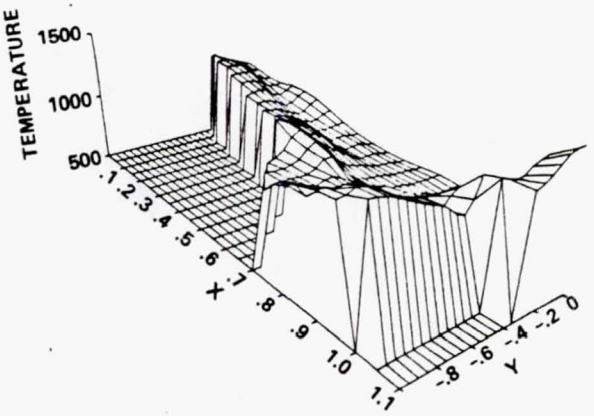


Fig. 9 DFI surface temperature distribution: STS-3 IRIS encounter.

telescope detector was 0.43 μW. Results like these are generated for all possible encounter points before an IRIS experiment.

IRIS Experiment Postflight

An example of the analytical registration method is displayed in Fig. 8. Here, the planform outline of the shuttle is projected onto the IRIS image plane. The flight environment data at the IRIS STS-3 encounter for both the shuttle and KAO aircraft, used to generate the projection, are given in Table 2. Note that the length of the orbiter's projection, from the nose to the end of the body flap, is about 7.5 mm. This is about 10% less than that of the IRIS image shown in Fig. 3. The analytical registration technique confirms and quantifies the conclusion reached with the original graphical technique: the IRIS image is spatially distorted. Moreover, the technique is useful in image restoration efforts.

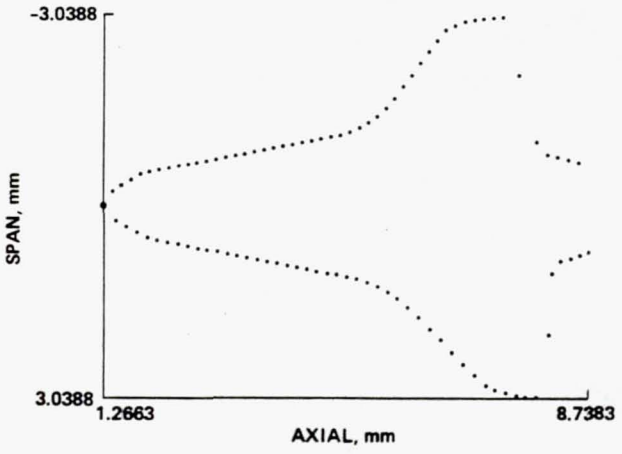


Fig. 8 Shuttle projection on IRIS image plane.

The DFI temperature distribution at the STS-3 IRIS encounter is plotted in Fig. 9. The area-averaged temperature is 1027 K, and the hemispherical emission, 4.4 MW. Using the IRIS geometry at acquisition time (16 sec before encounter), the fraction of the emitted signal detected by the acquisition telescope is 0.53 μW, which is similar to preflight estimate of 0.43 μW already discussed. The signal strength was, however, over three times the expected level. After some experimental testing, the IRIS Project Office determined that the discrepancy was caused by a problem in the radiometric calibration procedure. When the procedure was corrected, the actual signal strength agreed very well with the computed value.[7] The sensitivity of the acquisition telescope is three times greater than originally thought.

Detailed temperature comparisons of the IRIS image with the DFI are presented in Figs. 10. In Fig. 10a, the centerline temperatures compare fairly well in the midfuselage region, where the temperature gradients are small. But the image temperatures are markedly lower than the thermocouple measurements in the nose-cap and body-flap regions. In Fig. 10b, the 60% semispan temperatures on the wings are shown. The IRIS data are from the right wing, whereas the DFI are from the left. Since the temperature distribution is spanwise symmetric, the data can be compared. The comparison shows the same trends as that at the centerline, but with much more pronounced disagreement near the wing

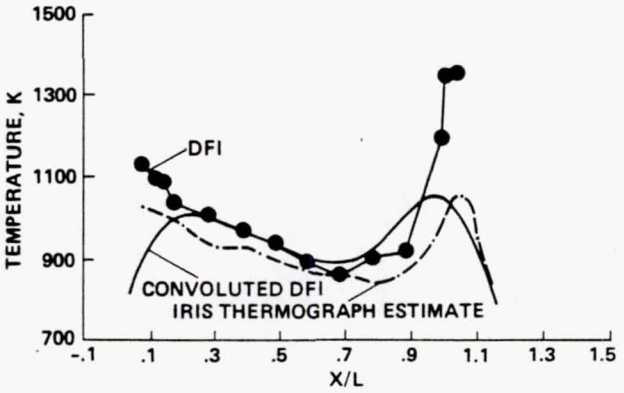


(a) Along centerline.

Fig. 10 Comparison of IRIS image with DFI temperatures and their convolution ($\sigma$ = 0.1).

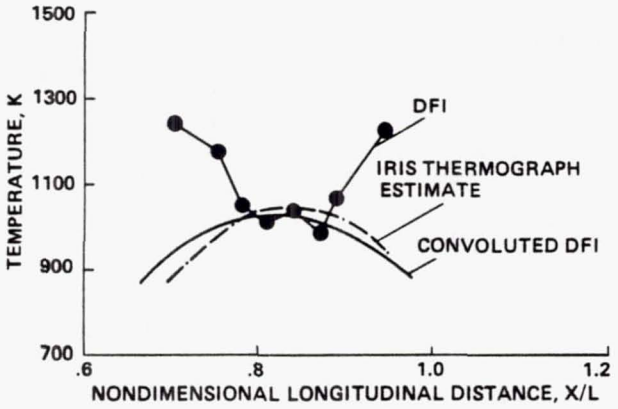


(b) Along wing at 60% semispan.

Fig. 10 Concluded.

leading edge and elevon trailing edge. Also shown in Figs. 10 are the results of convoluting the DFI distributions with a Gaussian density function having the standard deviation $\sigma$ equal to 10% of the shuttle length. Since the convolutions resemble, qualitatively, the image data, ground-based experiments onboard KAO aircraft were performed to check the focus of the IRIS optical system. The results showed that defocusing was not the major cause of the image degradation.

Flow-field results are compared with the DFI surface pressures at the STS-3 IRIS encounter in Fig. 11. The DFI pressure transducers are located near the nose at $X/L = 0.03$ at three circumferential positions on the left side of the orbiter. The pressures are selected for comparison because they are insensitive to real-gas effects. The trajectory and free-stream data used for the computation are listed in Table 2. Note that the flow-field solution is for a Mach number of 13 and an angle of attack of 40°. The computed pressure distribution is qualitatively similar to the measured values. The accuracy of the two measurements on the windward centerline is questionable because they occupy the same port, but they are 10% different. In the flow-field computation the surface temperature was assumed constant at 1200 K; this may also contribute to differences between the computed results and the flight data. The computations provide the shock-layer structure which is needed to assess its effect on the emitted infrared flux that produced the IRIS image.

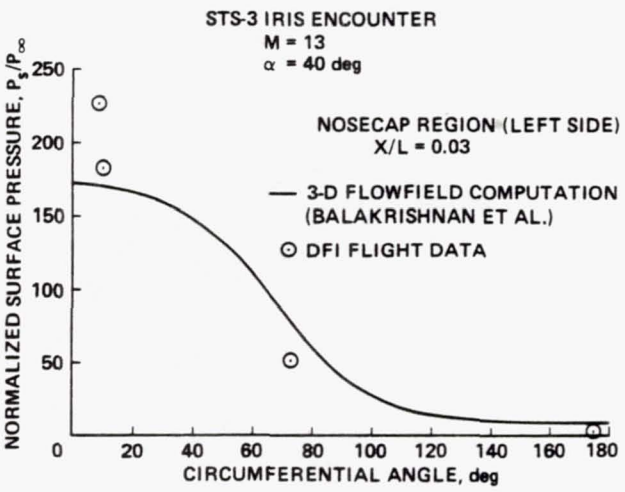


Fig. 11 Comparison of flow-field computation and DFI pressures at IRIS encounter.

The spatial and thermal distortions in the image have initiated an extensive investigation of the entire experiment by the IRIS Project Office. Laboratory tests have validated the IRIS hardware and data reduction software. William Davy, the IRIS Principal Technologist, has been working on isolating the physical phenomena that caused the distortions and on attempting to restore the degraded image.

Boundary-layer transition on the orbiter is of particular interest in shuttle aerothermodynamics. In fact, before the STS-3 landing was postponed for one day, the time during transitional heating was preselected as one of the prime IRIS encounter times. Figures 12 illustrate the starting and ending times of transition for various locations on the lower surface. The times are referenced to the start of transition at the location near the end of

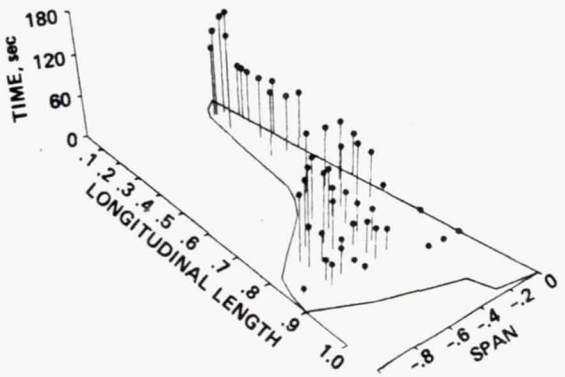


(a) Start.

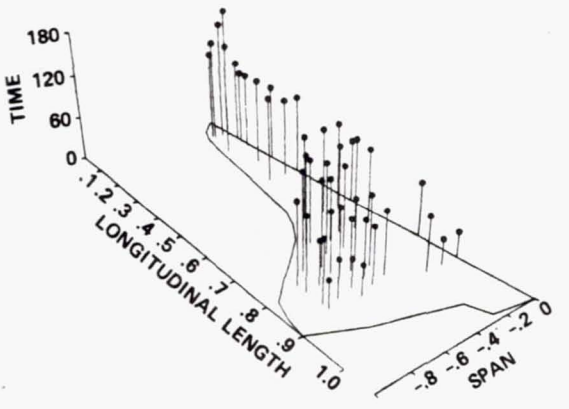


(b) End.

Fig. 12 Boundary-layer transition time distributions, STS-3, reference time = 1105 sec after EI.

the fuselage. At the reference time, M = 9.6, $Re_\infty = 6.6 \times 10^6$, and the angle of attack $\alpha = 37.5°$. Figure 12a gives the time when a particular location becomes transitional, that is, when the fully laminar heating regime has ended. It took 2 min for transitional zone to propagate to the nose-cap region. Figure 12b indicates the time when transition ends, that is, when the heating becomes fully turbulent. At a given location, the average duration in the transition zone is 30 sec. If the IRIS experiment continues, this transitional information will be useful in selecting an encounter point.

## CSE and TGH Experiments

The CSE and TGH experimental results for the STS-2 are presented in Figs. 13 and 14. CSE flight data, plotted in Fig. 13 and abstracted from Ref. 16, show that the baseline tiles are noncatalytic. The analytical theory developed by the CSE investigators compares well with the DFI data. Figure 14, taken from Ref. 13, compares the DFI data with the TGH heat-transfer analysis; the two agree favorably.

## Concluding Remarks

Computer software has been developed for processing the various data required to support the IRIS, CSE, and TGH Orbiter experiments sponsored by Ames Research Center. The application of this software to the first five STS missions has provided flight and ancillary data required for both pre- and post-data analysis of the experiments. The data have been helpful in detecting and correcting problems associated with the IRIS experiment, and in interpreting the STS-3 image. This data base will be useful in designing new experiments, extrapolating ground-based experimental results to flight conditions, and validating flow field and TPS response computer simulations. All of these findings will help in understanding the aerothermodynamic environment and the TPS response during repeated atmospheric entries for hypervelocity, the lifting vehicles like the Space Shuttle, and the future aero-assisted orbital transfer vehicle (AOTV), which is now in the conceptual design stage.


## Acknowledgments

We wish to thank W. Davy for his guidance and assistance in all phases of the work related to the IRIS experiment.


## References


[1]Jones, J. J., "OEX-Use of the Shuttle Orbiter as a Research Vehicle," AIAA Paper 81-2512, November 1981.

[2]Smith, J. A., "STS-3 Structural and Aerodynamic Pressure and Aerothermodynamic and Thermal Protection System Measurement Locations," NASA-JSC Report 17889, January 1982.

[3]Throckmorton, D. A., "Benchmark Aerodynamic Heat Transfer Data from the First Flight of the Space Shuttle Orbiter," AIAA Paper 82-0003, January 1982.

[4]Compton, H. R., Findlay, J. T., Kelly, G. M., and Heck, M. L., "Shuttle (STS-1) Entry Trajectory Reconstruction," AIAA Paper 81-2459, November 1981.


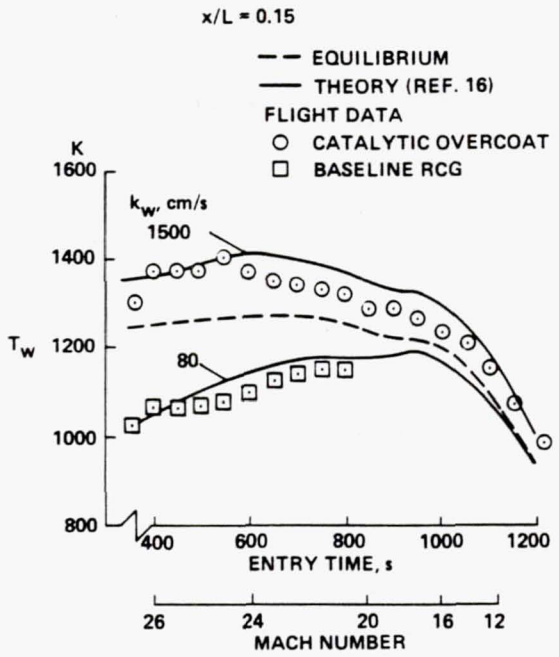


Fig. 13 Comparison of DFI flight data with CSE analysis, STS-2.

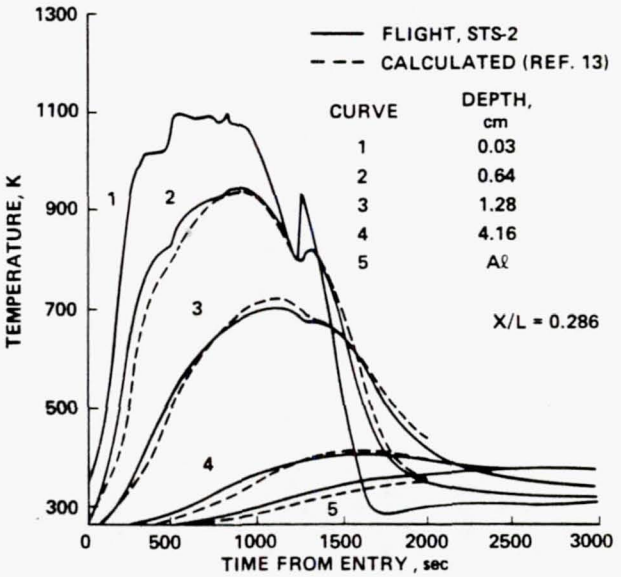


Fig. 14 Comparison of DFI flight data with TGH analysis, STS-2.

[5]Price, J. M. and Blanchard, R. C., "Determination of Atmospheric Properties for STS-1 Aerothermodynamic Investigations," AIAA Paper 81-2430, November 1981.

[6]Infrared Imagery of Shuttle (IRIS) Final Report," Martin Marietta Corp., Denver, Colorado, MCR-76-564, August 1977.

[7]Infrared Imagery of Shuttle (IRIS) Experiment: IRIS/STS-3 Engineering Report," Project Technology Branch, NASA Ames Research Center, Moffett Field, California, June 1982.

[8]Stewart, D. A., Rakich, J. V., and Lanfranco, M. J., "Catalytic Surface Effects Experiment on the Space Shuttle," AIAA Paper 81-1143, June 1981.

[9]Aviation Week and Space Technology, McGraw-Hill, Inc., New York, N.Y., April 12, 1982, p. 69.

[10]Britting, Kenneth R., Inertial Navigation Systems Analysis, Wiley-Interscience, New York, 1971.

[11]Pitts, W. C. and Murbach, M. S., "Flight Measurements of Tile Gap Heating on the Space Shuttle," AIAA Paper 82-0840, June 1982.

[12]Jung, E. J. Jr., "Mission Events List," NASA Johnson Space Center, December 1982.

[13]Rakich, J. V., Stewart, D. A., and Lanfranco, M. J., "Results of a Flight Experiment on the Catalytic Efficiency of the Space Shuttle Heat Shield," AIAA Paper 82-0944, June 1982.

| 1. Report No. | 2. Government Accession No. | 3. Recipient's Catalog No. |
|---|---|---|
| NASA TM-84345 | | |

| 4. Title and Subtitle | 5. Report Date |
|---|---|
| SUPPORTING FLIGHT DATA ANALYSIS FOR SPACE SHUTTLE ORBITER EXPERIMENTS AT NASA AMES RESEARCH CENTER | April 1983 |
| | 6. Performing Organization Code |

| 7. Author(s) | 8. Performing Organization Report No. |
|---|---|
| Michael J. Green,* Mari P. Budnick,† Lily Yang,† and Matthew P. Chiasson‡ | A-9289 |
| | 10. Work Unit No. |
| 9. Performing Organization Name and Address | 506-51-11 |
| *Ames Research Center, Moffett Field, Calif.; †Informatics General Corp., Palo Alto, Calif.; and ‡Foothill College, Los Altos, Calif. | 11. Contract or Grant No. |
| | 13. Type of Report and Period Covered |
| 12. Sponsoring Agency Name and Address | Technical Memorandum |
| National Aeronautics and Space Administration Washington, D.C. 20546 | 14. Sponsoring Agency Code |

15. Supplementary Notes

Point of Contact: Michael J. Green, Ames Research Center, M/S 229-41, Moffett Field, Calif. (415) 965-5389 or FTS 448-5389.

16. Abstract

The Space Shuttle Orbiter Experiments program is responsible for collecting flight data to extend the research and technology base for future aerospace vehicle design. The Infrared Imagery of Shuttle (IRIS), Catalytic Surface Effects, and Tile Gap Heating experiments sponsored by Ames Research Center are part of this program. The paper describes the software required to process the flight data which support these experiments. In addition, data analysis techniques, developed in support of the IRIS experiment, are discussed. Using the flight data base, the techniques have provided information useful in analyzing and correcting problems with the experiment, and in interpreting the IRIS image obtained during the entry of the third Shuttle mission.

| 17. Key Words (Suggested by Author(s)) | 18. Distribution Statement |
|---|---|
| Space Shuttle<br>OEX experiments | Unlimited<br><br>Subject Category - 18 |

| 19. Security Classif. (of this report) | 20. Security Classif. (of this page) | 21. No. of Pages | 22. Price* |
|---|---|---|---|
| Unclassified | Unclassified | 13 | A02 |

*For sale by the National Technical Information Service, Springfield, Virginia 22161